JOC The Journal of Organic Chemistry

Article

pubs.acs.org/joc

4′-*C*-[(4-Trifluoromethyl-1*H*-1,2,3-triazol-1-yl)methyl]thymidine as a Sensitive ^{19}F NMR Sensor for the Detection of Oligonucleotide Secondary Structures

Lotta Granqvist and Pasi Virta*

Department of Chemistry, University of Turku, 20014 Turku, Finland

Supporting Information

ABSTRACT: 4′-*C*-[(4-Trifluoromethyl-1*H*-1,2,3-triazol-1-yl)methyl]-thymidine was synthesized and incorporated as a phosphoramidite into oligonucleotide sequences. Its applicability as a sensor for the ^{19}F NMR spectroscopic detection of DNA and RNA secondary structures was demonstrated. On DNA, the ^{19}F NMR measurements were focused on monitoring of duplex−triplex conversion, for which this fluorine-labeled 2′-deoxynucleoside proved to be a powerful sensor. This sensor seemingly favors DNA, but its behavior in the RNA environment also turned out to be informative. As a demonstration, invasion of a 2′-*O*-methyl oligoribonucleotide into an RNA hairpin model (HIV-1 TAR) was monitored by ^{19}F NMR spectroscopy. According to the thermal denaturation studies by UV spectroscopy, the effect of the 4′-*C*-(4-trifluoromethyl-1*H*-1,2,3-triazol-1-yl)methyl moiety on the stability of these DNA and RNA models was marginal.

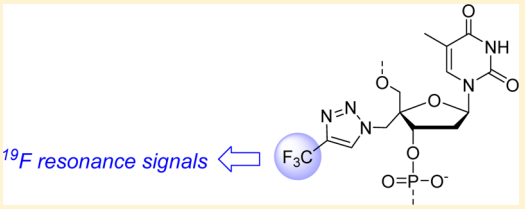

INTRODUCTION

Previous studies of ^{19}F NMR spectroscopy have shown it to be a promising tool for the characterization of molecular interactions, secondary structural arrangements, and their dynamics in oligonucleotides.[1−19] The sensitivity is still far from that of the conventional spectrophotometric measurements (UV, CD, and fluorescence-based techniques), but ^{19}F NMR may give more detailed information about the conversion mechanisms and relative mole fractions of the secondary structural species. The efficient discrimination even between only moderately different structures results from the wide chemical shift dispersion of the ^{19}F nucleus (50-fold compared to ^{1}H) and from the characteristic shift, which responds readily to changes in local van der Waals interactions and electrostatic fields.[19−23] It may even be suggested that once an appropriate label is readily available and its incorporation into oligonucleotides is facile, ^{19}F NMR measurements could be one of the routine methods for the characterization of molecular interactions and competing hybridization modes. In order to increase the sensitivity (83% of ^{1}H NMR sensitivity) and straightforwardness of the ^{19}F NMR measurement, there is an interest in developing nucleoside derivatives to which magnetically equivalent fluorine atoms (in a CF_3 group) are attached via an appropriate proton-coupling barrier [i.e., an isolated spin system provided by alkyne, thioether, or aryl bridges (cf. Figure 1); precisely, the CF_3 fluorines are magnetically equivalent only if their rotation rate is much faster than the effective correlation time of the nucleic acid structure]. These ^{19}F-multiplied sensors may allow rapid measurements at micromolar oligonucleotide concentrations without the need for ^{1}H decoupling techniques. The following obvious demands, which more or less compromise each other, should additionally be considered with the sensors: the effect on the native oligonucleotide structure should be marginal, while the resulting shift should clearly reflect the secondary structural changes. Examples of previously reported ^{19}F-multiplied sensors are presented in Figure 1. 5-[4,4,4-Trifluoro-3,3-bis(trifluoromethyl)but-1-ynyl]-2′-deoxyuridine (**1**), with nine equivalent fluorine atoms, has successfully been used for the detection of DNA and RNA double helices.[7,9,12] Although notable effects on the stabilities of the labeled DNA and RNA structures have not been observed, the bulky 4,4,4-trifluoro-3,3-bis(trifluoromethyl)but-1-ynyl group undeniably plays a dominating role in the major groove. 2′-Deoxy-5-(trifluoromethyl)uridine (**2**) is a commercially

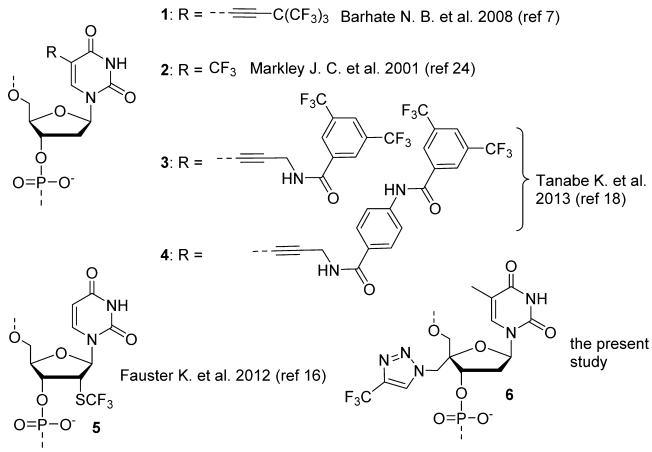

Figure 1. High-performance ^{19}F multiplied NMR sensors used for oligonucleotides.

Received: February 11, 2014
Published: March 28, 2014

   dx.doi.org/10.1021/jo500326j | J. Org. Chem. 2014, 79, 3529−3536

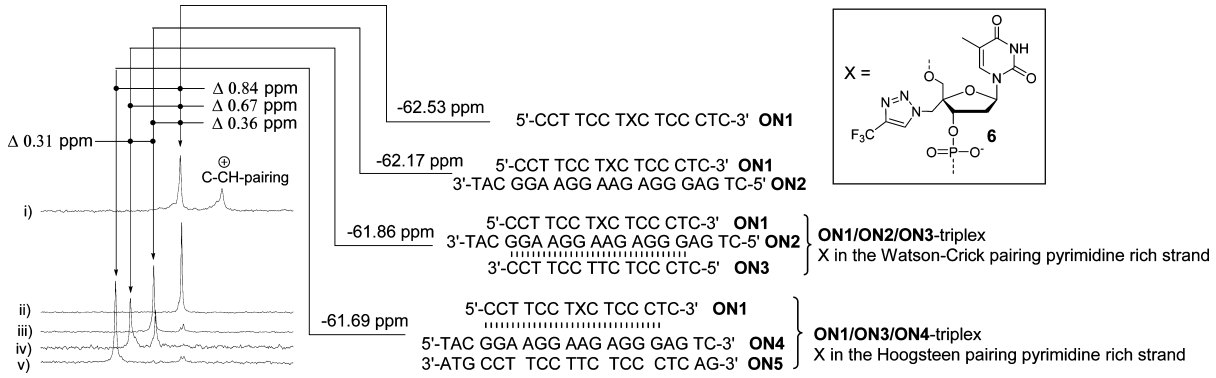

Figure 2. ^{19}F NMR signals of sensor **6** in different DNA hybrization modes. Conditions: (i) 100 μmol L^{-1} **ON1**, 10 mmol L^{-1} sodium phosphate (pH 5.5), 2 mmol L^{-1} $MgCl_2$, and 0.1 mol L^{-1} NaCl in D_2O–H_2O (1:9 v/v) at 25 °C; (ii) the same as (i) except at pH 6.0 and 37 °C; (iii) 50 μmol L^{-1} **ON1**, 45 μmol L^{-1} **ON2**, 10 mmol L^{-1} sodium phosphate (pH 6.0), 2 mmol L^{-1} $MgCl_2$, and 0.1 mol L^{-1} NaCl in D_2O–H_2O (1:9 v/v) at 37 °C; (iv) 50 μmol L^{-1} **ON1**, 50 μmol L^{-1} **ON2**, 50 μmol L^{-1} **ON3**, 10 mmol L^{-1} sodium phosphate (pH 6.0), 2 mmol L^{-1} $MgCl_2$, and 0.1 mol L^{-1} NaCl in D_2O–H_2O (1:9 v/v) at 50 °C, with the passive temperature-dependent shift eliminated and the shifts interpolated to that at 37 °C; (v) 100 μmol L^{-1} **ON1**, 100 μmol L^{-1} **ON3**, 100 μmol L^{-1} **ON4**, 10 mmol L^{-1} sodium phosphate (pH 6.0), 2 mmol L^{-1} $MgCl_2$, 0.1 mol L^{-1} NaCl in D_2O–H_2O (1:9 v/v) at 37 °C. (Note: in spite of the virtual homogeneity of the oligonucleotides, the shoulders of the ^{19}F NMR signals most likely originate from impurities.)

available nucleoside that has been incorporated into DNA double helices.[24] In spite of this modest base modification, a remarkable decrease in the duplex stabilities has been observed.[17,24] Additionally, this label is not compatible with the standard oligonucleotide protection scheme, since it is readily transformed to a 5-cyanouridine residue upon ammonolysis.[24] ^{19}F NMR applications with this potential sensor have not been described. Recently, 3,5-bis-(trifluoromethyl)benzoic acid (**3**) and 4-[3,5-bis-(trifluoromethyl)benzamido]benzoic acid (**4**) were postsynthetically coupled to 5-(3-aminopropyn-1-yl)-2′-deoxyuridine residues of oligonucleotide sequences, and the resulted sensors were used to probe mismatched and bulged DNAs by ^{19}F NMR spectroscopy.[18] Comparable to **1**, these sterically demanding major-groove-oriented base modifications do not remarkably retard hybridization with complementary oligonucleotides. Elegant ^{19}F NMR applications (structure probing of bistable RNA, characterization of RNA–protein and RNA–small-molecule interactions) using 2′-deoxy-2′-trifluoromethylthiouridine (**5**) as a sensor have been described.[16] The synthesis of phosphoramidite derivative **5** and its incorporation into an RNA sequence were straightforward, and the resulting ^{19}F NMR shift of the sensor clearly distinguished between different secondary structures. With this sensor, however, a clearly facilitated thermal denaturation (57 vs 72 °C) of an RNA hairpin was reported.

In response to the above demands, a novel 4′-*C*-modified ^{19}F NMR sensor, 4′-*C*-[(4-trifluoromethyl-1*H*-1,2,3-triazol-1-yl)-methyl]thymidine (**6**), is described in the present report. This sensor (as a deoxynucleoside with predominant *S* conformation) was primarily designed for the detection of DNA secondary structures, which was demonstrated by the ^{19}F NMR spectroscopic monitoring of DNA triplex/duplex/single strand conversion. For these experiments **6** proved to be an excellent sensor, resulting in sharp and well-distinguished ^{19}F signals as unique singlets for DNA triplexes (**6** paired via both the Watson–Crick face and the Hoogsteen face), a DNA duplex, and a single strand (Figure 2). **6** turned out to be informative also for the RNA environment. Three different sites of an HIV-1 trans-activation response element (TAR) RNA model were labeled by **6**, and our previously reported study of ^{19}F NMR spectroscopic characterization of RNA invasion[9] was repeated and confirmed. The 4-trifluoromethyl-1*H*-1,2,3-triazol-1-yl group offered a quasi-isolated spin system in a similar manner as a trifluoromethylphenyl group (cf. **3** and **4**), and ^{19}F NMR data could be obtained without the need for fluorine–proton decoupling. The effect of sensor **6** on the stability of these DNA and RNA models was marginal, although it expectedly depended slightly on the labeling site (Table 1).

Table 1. UV Melting Temperatures (T_m) of the ^{19}F-Labeled Secondary Structures of Oligonucleotides (X = 6) and Values of ΔT_m in Comparison with Unmodified Oligonucleotides (X = Thymidine or Uridine)[a]

entry	oligonucleotides labeled with **6**	T_m/°C (ΔT_m/°C)
1	**ON1**/**ON2** duplex	54.9 (−0.6)
2	**ON1**/**ON2**/**ON3** triplex	32.9 (−0.6)
3	**ON1**/**ON4**/**ON5** triplex	31.0 (−1.7)
4	**^{19}F-HIV-1 TAR(1)**	72.4 (+0.5)
5	**^{19}F-HIV-1 TAR(2)**	71.0 (−0.9)
6	**^{19}F-HIV-1 TAR(3)**	69.2 (−2.7)

[a]Conditions: 10 mmol L^{-1} NaH_2PO_4 (pH 6.0), 0.1 mol L^{-1} NaCl, 2.0 mmol L^{-1} $MgCl_2$, and 2.0 μmol L^{-1} each oligonucleotide (entries 1–3); 10 mmol L^{-1} sodium cacodylate (pH 7.0), 0.1 mol L^{-1} NaCl, and 2.0 μmol L^{-1} each oligonucleotide (entries 4–6).

RESULTS AND DISCUSSION

4′-*C*-[(4-Trifluoromethyl-1*H*-1,2,3-triazol-1-yl)methyl]-thymidine Sensor 6 and Synthesis of Its Phosphoramidite Derivative 12. The 4′-C is an attractive site for the introduction of a label in DNA. Previous studies have shown that the 4′-modification faces the minor groove upon hybridization, and oligonucleotides modified at this site usually form equally stable double helices compared with their unmodified counterparts.[25−34] It may also be expected that the fluorine label at this site in **6** only marginally disturbs the secondary structure of DNA but is sensitive to secondary structural arrangements because of the particular orientation. The 4′-C additionally is a uniform site for the label compared with, for example, the base-modified probes **1**–**4**. On RNA,

dx.doi.org/10.1021/jo500326j | J. Org. Chem. 2014, 79, 3529–3536

however, certain shortcomings of **6** may be expected: **6** lacks the 2′-OH group, and the predominant *S* conformation may disfavor A-type helices. Additionally, on an RNA duplex the (4-trifluoromethyltriazolyl)methyl group at the 4′-C position is oriented outward from the helix, not onto the edge of the minor groove as in DNA, and hence, only modest ^{19}F NMR spectroscopic discrimination between double-stranded and single-stranded RNA may be expected. In spite of these presumptions, the behavior of **6** in the RNA environment proved promising (Table 1; also see Figures 5 and 6 below). The 4′-trifluoromethyl-1*H*-1,2,3-triazol-1-yl moiety was chosen because it may be readily obtained from the corresponding azide derivative **10**[33] (note: the triazolyl moiety is a weak base,[35] which is entirely uncharged in the ^{19}F NMR measurements used for the oligonucleotides below) via copper(I)-catalyzed Huisgen 1,3-dipolar cycloaddition.[36,37] A high-yielding procedure for the preparation of 4′-*C*-azidomethyl-3′-*O*-(4,4′-dimethoxytrityl)thymidine (**10**) (Scheme 1) was

Scheme 1. Synthesis of Phosphoramidite Building Block 12[a]

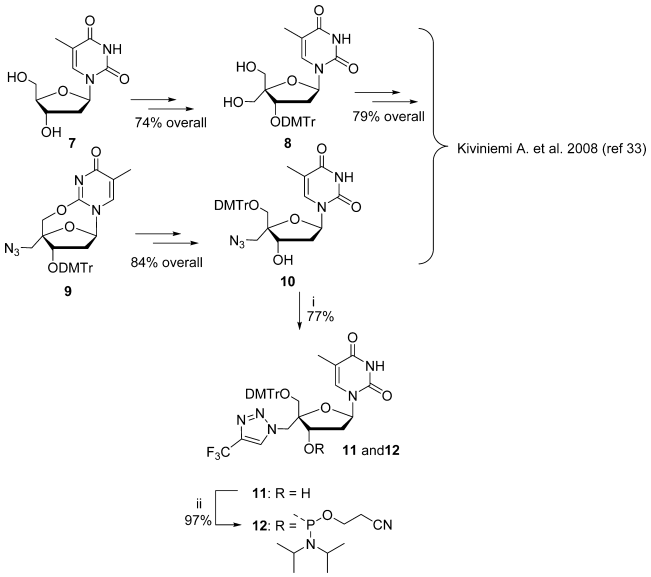

[a]Conditions: (i) 3,3,3-trifluoroprop-1-yne, $CuSO_4$, sodium ascorbate; (ii) 2-cyanoethyl *N*,*N*-diisopropylphosphoramidochloridite, Et_3N, DCM.

previously reported.[33,38] Accordingly, 4′-*C*-hydroxymethylthymidine **8** was first synthesized from thymidine (**7**) following the literature procedure.[38,39] The primary hydroxyl groups were converted to triflates and then the $O^{2,5'}$-anhydronucleoside was formed,[40] after which the remaining 4′-*C*-trifluoromethanesulfonyl group was replaced with azide ion to give **9**. The anhydronucleoside bridge was hydrolyzed, the 3′-OH group exposed, and the 5′-OH group protected with a DMTr group. Several synthetic steps were required, but the procedure was reproducible and the overall yield from **7** to **10** was relatively high (49%). Copper(I)-catalyzed Huisgen 1,3-dipolar cycloaddition[36] between the 4′-*C*-azidomethyl group of **10** and gaseous 3,3,3-trifluorobutyne gave **11** with the trifluoromethyltriazolyl moiety in 77% yield, and the 3′-OH group was then quantitatively (97%) phosphitylated to afford the desired phosphoramidite **12**. The above-described synthesis of 4′-C modification evidently may be generalized for other nucleosides, but the fact should be borne in mind that the correct stereocontrol for the 4′-C substituent is facile only in thymidine. The anhydronucleoside **9**[40] determined the stereocontrol.

Oligonucleotide Synthesis. Oligonucleotides were synthesized on a 1.0 μmol scale using an automatic DNA/RNA synthesizer. Benzylthiotetrazole as an activator and coupling times of 20 and 300 s were used for the couplings of standard DNA and RNA building blocks, respectively. For the fluorine-labeled thymidine phosphoramidite **12** (using a 0.13 mol L^{-1} solution in dry MeCN to load the reagent vessel), the coupling time was increased to 600 s, resulting in a coupling efficiency of 92%. Nearly quantitative coupling of **12** could be provided by repeating the automatic coupling step or by using a manual phosphoramidite coupling in which a more concentrated solution (final concentration 0.11 mol L^{-1} after addition of the activator) but a smaller excess (10 equiv) of **12** could be used (see the Experimental Procedures). Otherwise, standard DNA and RNA protocols were applied. The oligonucleotides were released from the support with concentrated ammonia (33% aqueous NH_3 at 55 °C overnight), and TBDMS protections were removed by treatment with triethylamine trihydrofluoride followed by filtration through an ion exchange cartridge. The purification was carried out by RP HPLC. According to the RP HPLC profiles (see the Supporting Information), only a slight decrease in the purities of the labeled sequences compared with that of the unlabeled sequence was observed. The authenticity of the oligonucleotides was verified by MS (ESI-TOF).

^{19}F NMR Measurements. Instead of testing probe **6** for new, sophisticated ^{19}F NMR applications, its behavior was demonstrated in relatively well studied and defined secondary structures: in a DNA duplex, in DNA triplexes (**6** paired via both the Hoogsteen face and the Watson−Crick face), and in HIV-1 TAR models upon invasion with 2-*O*-methyl oligoribonucleotides in which three different sites were labeled: (1) the stem region before the bulge, (2) the stem region between the loop and the bulge, and (3) the loop. In this manner we also could get rather comprehensive understanding of how this sensor affects the stabilities of native oligonucleotide structures in varying local environments of the sensor (Table 1).

As a first example, we repeated the experiment previously reported by Tanabe et al.[10] They used 5-fluoro-2′-deoxyuridine as an ^{19}F signal transmitter for the detection of triplex formation between **ON1**, **ON4**, and **ON5** (Figure 3). In contrast to their experiments, lower oligonucleotide concentrations of 50 and 100 μmol L^{-1} (vs 250 μmol L^{-1}) and a higher pH of 6.0 (vs 5.5) were used for the triplex formation. At 25 °C and pH 5.5, **ON1** (100 μmol L^{-1}, X = 4′-*C*-[(4-trifluoromethyl-1*H*-1,2,3-triazol-1-yl)methyl]thymidine, 10 mmol L^{-1} sodium phosphate, 2 mmol L^{-1} $MgCl_2$, 0.1 mol L^{-1} NaCl) appeared as two signals in the ^{19}F NMR spectrum (i in Figure 2), as described by Tanabe et al.[10] The sharp signal at −62.53 ppm referred to the single strand, and the broad signal ca. 0.6 ppm upfield resulted from unspecific C−CH^+ quartets (but not necessarily from a specific i motif). At a higher pH of 6.0 (at 37 °C), only the sharp signal at −62.53 ppm was detected (ii in Figure 2). The triplex formation was then carried out (I in Figure 3). **ON1** was titrated with **ON4**/**ON5** duplex, which should result in binding of **ON1** via the Hoogsteen face. As shown in I in Figure 3, clear conversion of the initial signal at −62.53 ppm to a new sharp signal at −61.69 ppm occurred, which indicated **ON1**/**ON4**/**ON5** triplex formation. Since sharp and well-distinguished signals ($\Delta\delta$ = 0.83 ppm) were

dx.doi.org/10.1021/jo500326j | J. Org. Chem. 2014, 79, 3529−3536

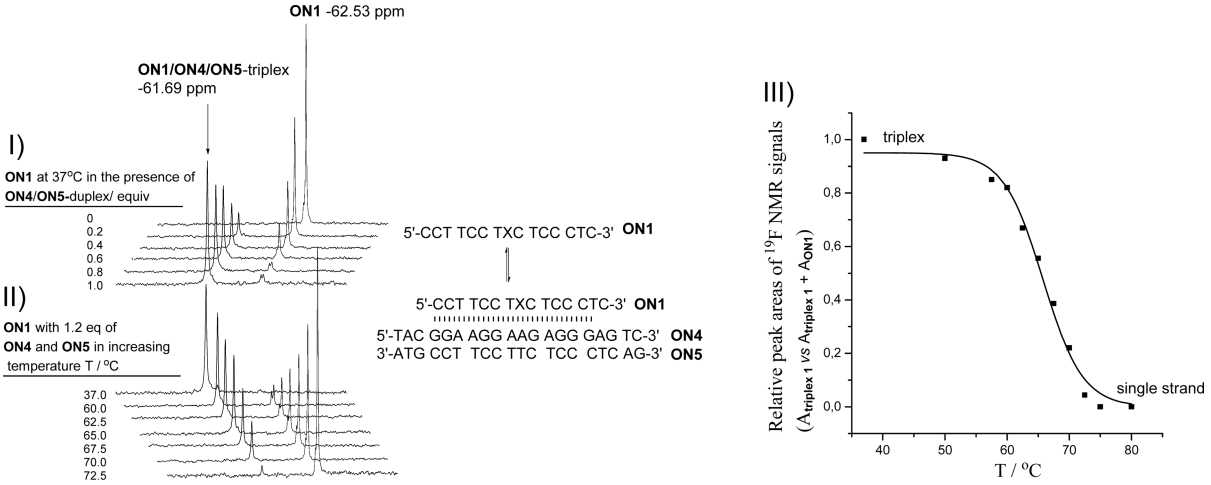

Figure 3. (I) Formation and (II, III) thermal melting of the **ON1**/**ON4**/**ON5** DNA triplex followed by ^{19}F NMR spectroscopy. Conditions: 100 μmol L^{-1} **ON1**, 0−120 μmol L^{-1} **ON4** and **ON5** (1:1 mol/mol), 10 mmol L^{-1} sodium phosphate (pH 6.0), 2 mmol L^{-1} $MgCl_2$, and 0.1 mol L^{-1} NaCl in D_2O−H_2O (1:9 v/v).

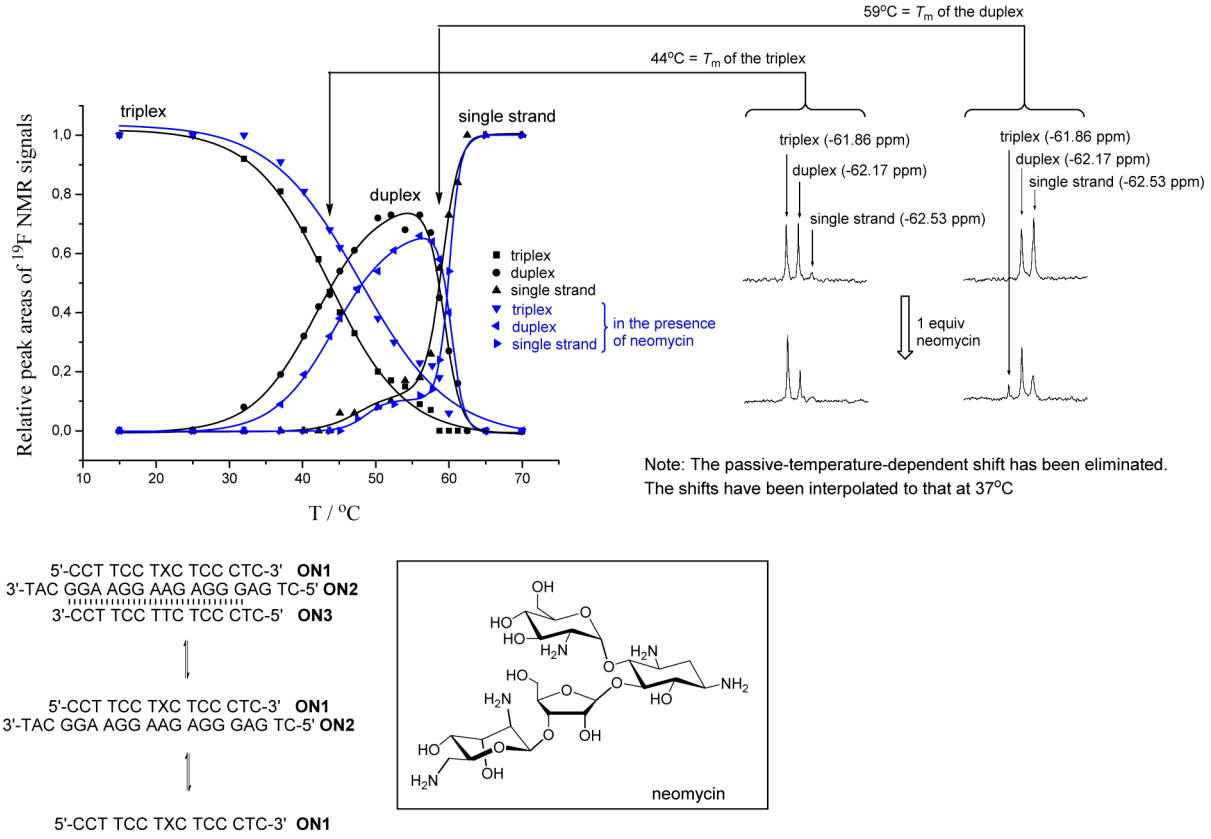

Figure 4. DNA triplex/duplex/single strand conversions followed by ^{19}F NMR spectroscopy. Conditions: 50 μmol L^{-1} **ON1**, **ON2**, and **ON3**, 10 mmol L^{-1} sodium phosphate (pH 6.0), 2 mmol L^{-1} $MgCl_2$, and 0.1 mol L^{-1} NaCl in D_2O−H_2O (1:9 v/v).

detected, we next studied whether the relative peak areas at increasing temperature (II in Figure 3) could be applied to the determination of the melting temperature (T_m) of the **ON1**/**ON4**/**ON5** triplex. As shown, a nice negative S curve was obtained (III in Figure 3), in which the inflection point at 66 °C showed thermal melting. [The difference between the T_m values in 100 μmol L^{-1} (66 °C) and 2 μmol L^{-1} (31.0 °C) solutions of oligonucleotides should be noted (Table 1)].

The ^{19}F NMR spectroscopic behavior of the sensor was then similarly studied upon formation of the **ON1**/**ON2** duplex and the **ON1**/**ON2**/**ON3** triplex. Sharp and unique signals resulted also for these secondary structures at −62.17 and −61.86 ppm, respectively (Figure 2; the more detailed data of the titrations are not presented). Melting of the **ON1**/**ON2**/**ON3** triplex bearing the sensor in the Watson−Crick face was more informative than that of **ON1**/**ON4**/**ON5** triplex (Figure 4). As shown, the conversion from the **ON1**/**ON2**/**ON3** triplex to the **ON1**/**ON2** duplex and finally to the **ON1** single strand could be nicely followed according to the relative peak areas of the ^{19}F NMR resonance signals. The oligonucleotide

dx.doi.org/10.1021/jo500326j | J. Org. Chem. 2014, 79, 3529−3536

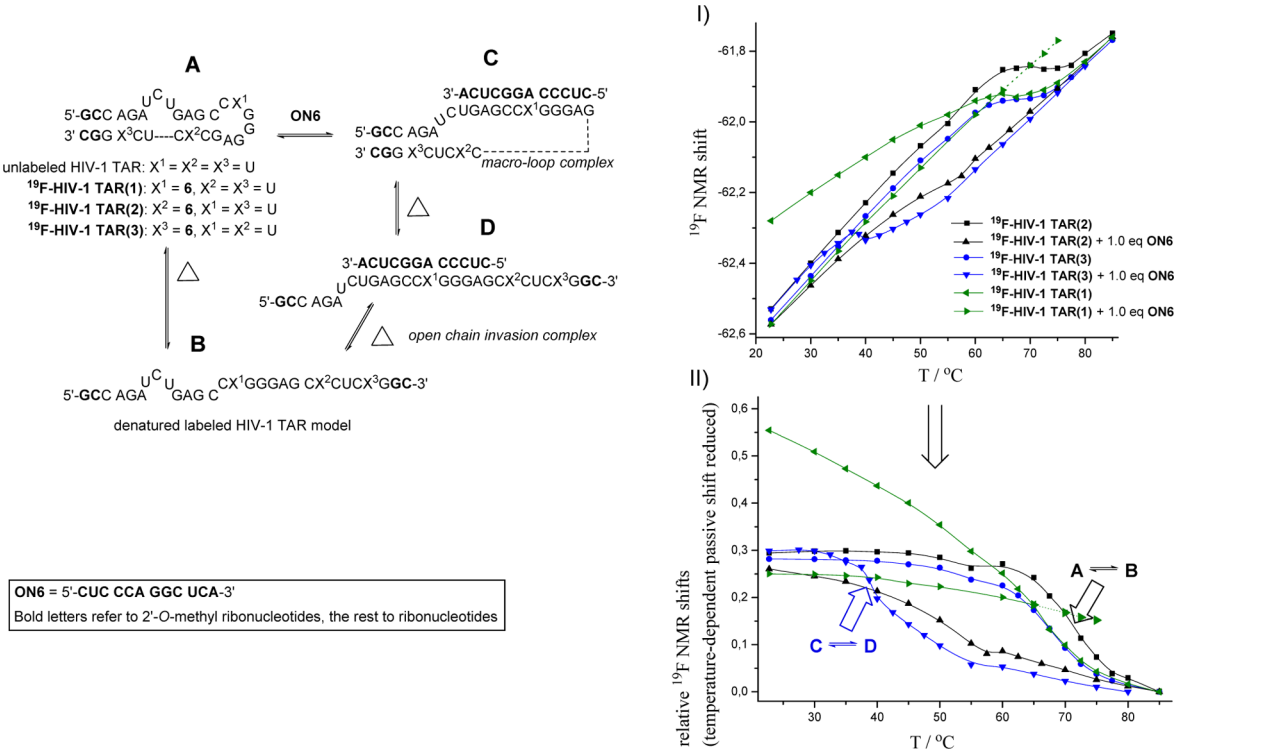

Figure 5. ^{19}F NMR shift-vs-temperature profiles of ^{19}F-labeled HIV-TAR models and their invasion complexes. Conditions: 50 μmol L^{-1} labeled **^{19}F-HIV-1 TAR(1−3)** with and without 50 μmol L^{-1} **ON6**, 10 mmol L^{-1} sodium cacodylate (pH 7.0), and 0.1 mol L^{-1} NaCl in D_2O−H_2O (1:9 v/v).

concentration in this experiment was 50 μmol L^{-1}. It may be worth mentioning that a seemingly direct conversion of the **ON1**/**ON2**/**ON3** triplex to **ON1** was observed at a concentration of 100 μmol L^{-1} (in our initial attempt), which was a result of the stronger concentration dependence of the triplex compared with the duplex.

Triple helices may be stabilized by aminoglycosides.[41−43] Among them, neomycin has proven to be the most effective ligand. The above-described triplex/duplex/single strand conversion was followed also in the presence of neomycin (Figure 4, blue curves). As shown, 1.0 equiv of neomycin was enough to stabilize the **ON1**/**ON2**/**ON3** triplex (50 μmol L^{-1}) clearly (ΔT_m = 4 °C), whereas the **ON1**/**ON2** duplex was less stabilized. The difference between these stabilizations was consistent with the literature.[41−43] Oligonucleotides have been conjugated to aminoglycosides in order to increase their affinities to RNA targets,[12,33,34,44,45] but attempts to use them for triplex recognition have failed to date. However, the approach may still have some potential, since the observed enhanced triplex formation shown in Figure 4 resulted from only a stoichiometric amount of neomycin.

We previously used ^{19}F NMR spectroscopy to characterize the invasion of 2′-*O*-methyl oligoribonucleotides to an ^{19}F-labeled HIV-1 TAR model,[9] and later the same experiment was applied for the verification of aminoglycoside-enhanced invasion.[12] In these previous reports, sensor **1**[7] was incorporated into the tetranucleotide stem region between the bulge and the loop of an HIV-1 TAR model [cf. **^{19}F-HIV-1 TAR(2)** in Figure 5 with X^2 = **1** and X^1 = X^3 = U], and it was able to detect not only the denaturation of HIV-1 TAR but also the conversion of the macro-looped complex to the open-chain invasion complex (cf. structures A, B, C, and D in Figure 5). Interestingly, separate, albeit partially coalescent, signals for the A/B and C/D equilibria were observed, which indicated that rearrangements between these structures were slow on the NMR time scale. For intramolecular hybridizations, the equilibrium is usually fast on the NMR time scale,[6] which questions our previous conclusions.

In the present study, **6** was incorporated at three different positions of the same HIV-1 TAR model (X^1, X^2, and X^3 in **^{19}F-HIV-1 TAR(1)**, **^{19}F-HIV-1 TAR(2)** and **^{19}F-HIV-1 TAR(3)**, respectively; Figure 5), and the RNA invasion studies were repeated. ^{19}F NMR measurements were carried out using oligonucleotide concentrations of 50 μmol L^{-1} in 0.10 mol L^{-1} NaCl buffered by 10 mmol L^{-1} sodium cacodylate, pH 7.0 (previous conditions: 20 μmol L^{-1} ^{19}F-labeled HIV-1 TAR with **ON6** in 0.1 mol L^{-1} NaCl with 25 mmol L^{-1} NaH_2PO_4, pH 6.5). The thermal UV melting temperatures for the HIV-1 TAR models under these experimental conditions (69.2−72.4 °C) are listed in Table 1. The ^{19}F NMR spectra of each labeled HIV-1 TAR model with and without 1.0 equiv of **ON6** were measured at varying temperatures. The ^{19}F NMR shift-versus-temperature profiles are presented in I in Figure 5, and the profiles of the shift differences versus temperature after reduction of the passive temperature-dependent shift are shown in II in Figure 5. The thermal melting of HIV-1 TAR (A/B equilibrium) could be monitored by the stem-located sensors (X^2 and X^3) as negative S curves (■, ●), while **6** in the loop (X^1) shifted continuously (◀ over 0.5 ppm) over the whole temperature range measured (23−75 °C). In comparison to the UV melting profiles (Table 1), slightly different T_m values were obtained from the ^{19}F NMR shift-versus-temperature profiles, given by the inflection points at 71 °C for **^{19}F-HIV-1 TAR(2)** and at 68 °C for **^{19}F-HIV-1 TAR(3)** (II in Figure 5). It is worth noting that now well-behaving coalescence signals were obtained [see the spectra of **^{19}F−**

dx.doi.org/10.1021/jo500326j | J. Org. Chem. 2014, 79, 3529−3536

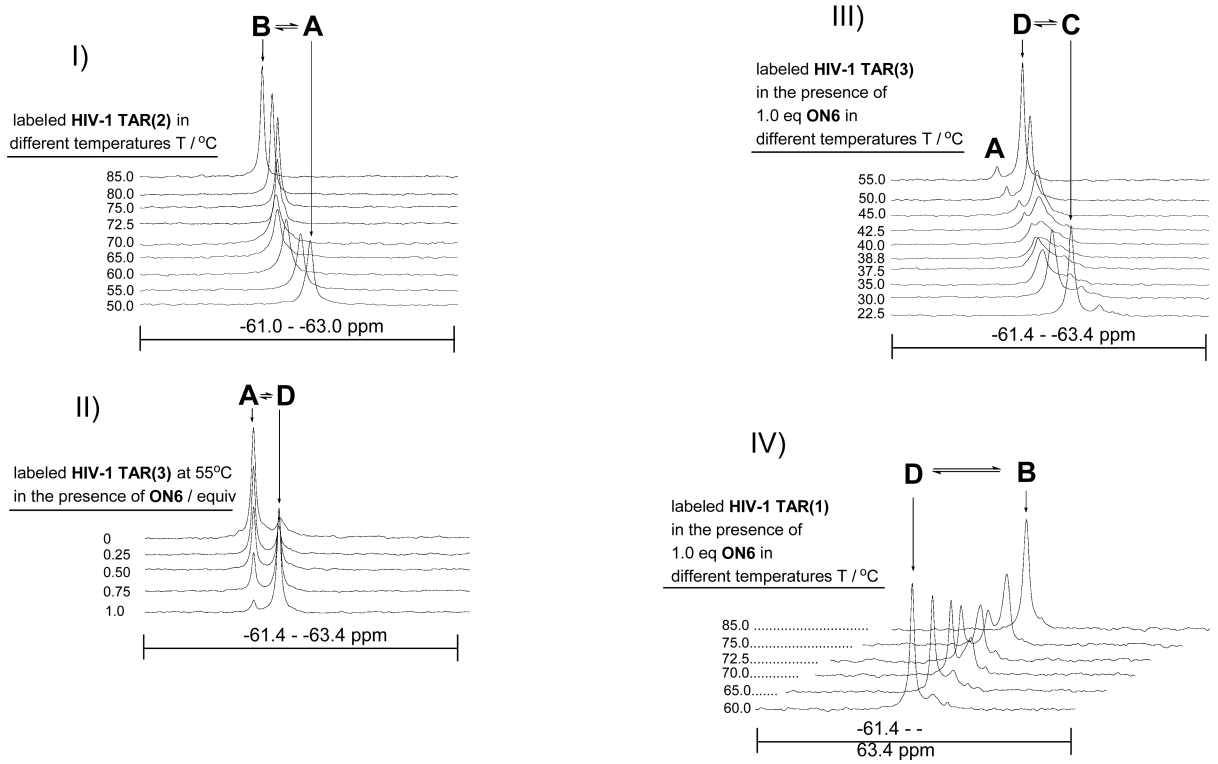

Figure 6. ^{19}F NMR spectra of ^{19}F-labeled HIV-TAR models and their invasion complexes in increasing temperature. Conditions: 50 μmol L^{-1} labeled **^{19}F-HIV-1 TAR(1−3)** with and without 50 μmol L^{-1} **ON6** (titration carried out in II), 10 mmol L^{-1} sodium cacodylate (pH 7.0), and 0.1 mol L^{-1} NaCl in D_2O−H_2O (1:9 v/v) (cf. the shift data in Figure 5).

HIV-1 TAR(2) in panel I of Figure 6]. Thus, it seems that a heavily modified sensor such as **1**, even if it does not decrease the stability of the secondary structure, may misrepresent the rate of denaturation. The equilibrium between the macro-loop invasion complex (C) and the open-chain invasion complex (D) could be monitored by labeled **^{19}F-HIV-1 TAR(3)** (X^3 = **6**, X^1 = X^2 = U). Also here, an averaged signal between the structures was obtained, but the signal was broad (III in Figure 6). The incomplete coalescence signal refers to a slower process in comparison with the hairpin melting (A/B). The inflection point at 39 °C in the shift-versus-temperature profile (▼), corresponding to T_m of the macro-loop complex C, is clearly seen. **6** in **^{19}F-HIV-1 TAR(2)** (X^2 = **6**, X^1 = X^3 = U) also reflected the C/D equilibrium, but an unclear shift-versus-temperature profile was obtained (▲). As shown in II in Figure 5, the signals of the hairpin HIV-1 TAR (A) and the macro-loop complex C overlapped, but the titration with **ON6** could be followed at 55 °C (i.e., under conditions where A was directly converted to the open-chain invasion complex D; II in Figure 6). Finally, melting of the open-chain invasion complex D to give the denatured HIV-1 TAR (B) could be followed by relative ^{19}F NMR peak areas using **^{19}F-HIV-1 TAR(1)** (X^1 = **6**, X^2 = X^3 = U) (IV in Figure 6). As shown by these results, the ^{19}F shift difference between the signals of the single-stranded and double-stranded RNA was only slightly smaller than that with DNA, and invasion of a 2′-*O*-methyl oligoribonucleotide into a HIV-1 TAR model and its mechanism could be clearly characterized by ^{19}F NMR spectroscopy using **6** as a signal transmitter (Figures 5 and 6).

CONCLUSION

A new ^{19}F-multiplied sensor for the ^{19}F NMR spectroscopic detection of oligonucleotide secondary structures, 4′-*C*-[(4-trifluoromethyl-1*H*-1,2,3-triazol-1-yl)methyl]thymidine (**6**), has been described. The synthesis of the corresponding phosphoramidite building block **12** was straightforward, and it was readily incorporated into DNA and RNA sequences by an automatic synthesizer. The uniform 4′-C position for the fluorine sensor proved to behave nicely in DNA and RNA environments. In ^{19}F NMR spectroscopy, **6** readily reflected secondary structural arrangements but only slightly affected the stabilities compared with the native oligonucleotide structures (as verified by UV melting profiles). ^{19}F NMR spectroscopic characterization of DNA triplex/duplex/single strand conversion and of invasion of an RNA hairpin model (HIV-1 TAR) was demonstrated.

EXPERIMENTAL PROCEDURES

General Remarks. Dichloromethane and MeCN were dried over 4 Å molecular sieves, and triethylamine was dried over CaH_2. NMR spectra were recorded at 500 MHz. The chemical shifts for ^{1}H and ^{13}C NMR are given in parts per million from the residual signals of the deuterated solvents (CD_3OD and CD_3CN). ^{31}P NMR shifts are referenced to external H_3PO_4 and ^{19}F NMR shifts to external CCl_3F. Mass spectra were recorded using electrospray ionization (ESI).

5′-*O*-(4,4′-Dimethoxytrityl)-4′-*C*-[(4-trifluoromethyl-1*H*-1,2,3-triazol-1-yl)methyl]thymidine (11). To a mixture of 4′-*C*-azidomethyl-5′-*O*-(4,4′-dimethoxytrityl)thymidine (**10**)[33] (0.86 g, 1.4 mmol) in DMSO (6 mL) were added aqueous solutions of $CuSO_4$ (0.1 mol L^{-1}, 150 μL, 15 μmol) and sodium ascorbate (0.1 mol L^{-1}, 1.5 mL, 0.15 mmol). The reaction was carried out in a sealed tube placed in an ice bath and bubbled with gaseous 3,3,3-trifluoropropyne for 5 min. The reaction mixture was then stirred at room temperature for 48 h, during which time the gas was added three times in an ice

dx.doi.org/10.1021/jo500326j | J. Org. Chem. 2014, 79, 3529−3536

bath along with additions of the aqueous solutions of $CuSO_4$ (100 μL, 10 μmol) and sodium ascorbate (400 μL, 40 μmol). The reaction mixture was then partitioned between dichloromethane and water. The organic phase was separated, dried over Na_2SO_4, and evaporated to dryness. The residue was purified by silica gel chromatography (30−0% hexane and 0.1% Et_3N in EtOAc) to yield 0.77 g (77% yield) of **11** as a yellowish oil. ^{1}H NMR (500 MHz, CD_3OD) δ: 8.38 (s, 1H), 7.43 (s, 1H), 7.40−7.38 (m, 2H), 7.28−7.19 (m, 7H), 6.82−6.81 (m, 4H), 6.43 (dd, 1H, *J* = 7.3 and 6.1 Hz), 4.88 (d, 1H, *J* = 14.7 Hz), 4.79−4.76 (m, 2H), 3.74 (s, 6H), 3.25 (d, 1H, *J* = 10.3 Hz), 2.87 (d, 1H, *J* = 10.3 Hz), 2.44 (m, 1H), 2.33 (ddd, 1H, *J* = 13.7, 6.1, and 3.1 Hz), 1.42 (s, 3H). ^{13}C NMR (125 MHz, CD_3OD) δ: 164.8, 159.0, 158.9, 150.9, 144.3, 137.8 (q, *J* = 39.0 Hz), 136.1, 135.0, 134.7, 130.0, 127.9, 127.6, 126.8, 125.9, 120.7 (q, *J* = 266.7 Hz), 112.8, 110.6, 87.3, 86.4, 84.5, 72.1, 64.1, 54.3, 52.0, 39.6, 10.7. ^{19}F NMR (470 MHz, CD_3OD) δ: −63.64. HRMS (ESI-TOF) *m/z*: calcd for $C_{35}H_{34}F_3N_5NaO_7$ $[M + Na]^+$ 716.2308, found 716.2310.

3′-*O*-[(2-Cyanoethoxy)-(*N*,*N*-diisopropylamino)phosphinyl]-5′-*O*-(4,4′-dimethoxytrityl)-4′-*C*-[(4-trifluoromethyl-1*H*-1,2,3-triazol-1-yl)methyl]thymidine (12). Compound **11** (0.15 g, 0.22 mmol) was dried over P_2O_5 in a vacuum desiccator and dissolved in dry dichloromethane (1.5 mL). Triethylamine (152 μL, 1.1 mmol) and 2-cyanoethyl *N*,*N*-diisopropylphosphoramidochloridite (78 μL, 0.35 mmol) were added, and the mixture was stirred under nitrogen for 2 h. Upon completion of the reaction, the reaction mixture was eluted through a short dried silica gel column (60−0% hexane and 0.1% Et_3N in EtOAc) to yield two diastereomers of **12** as white foams (overall 0.19 g, 97% yield). *Diastereomer I*: ^{1}H NMR (500 MHz, CD_3CN) δ: 9.36 (b, 1H), 8.22 (s, 1H), 7.45−7.25 (m, 10H), 6.88 (m, 4H), 6.34 (dd, ^3J = 6.7 Hz average), 5.01 (m, 1H), 4.85 (d, 1H, ^2J = 14.9 Hz), 4.74 (d, 1H, ^2J = 14.9 Hz), 3.87−3.76 (m, 2H), 3.79 and 3.78 (both s, 6H), 3.73−3.66 (m, 2H), 3.24 (d, 1H, ^2J = 10.4 Hz), 2.93 (d, 1H, ^2J = 10.4 Hz), 2.63 (m, 2H), 2.47−2.37 (m, 2H), 1.52 (segmented, 3H), 1.25−1.23 (m, 12H). ^{13}C NMR (125 MHz, CD_3CN) δ: 163.7, 158.9, 150.3, 144.5, 137.5 (q, *J* = 38 Hz), 135.8, 135.2, 135.0, 130.1, 128.0, 127.1, 126.0, 120.9 (q, *J* = 265 Hz), 118.4, 113.2, 110.5, 87.0, (85.79 and 85.75), 84.2, (74.2 and 74.0), 63.4, (58.8 and 58.6), 54.9, 52.2, (43.2 and 43.1), 38.2, (24.97 and 23.91), (20.1 and 20.0), 11.2. ^{31}P NMR (200 MHz, CD_3CN) δ: 149.8. ^{19}F NMR (470 MHz, CD_3CN) δ: −63.28. *Diastereomer II*: ^{1}H NMR (500 MHz, CD_3CN) δ: 9.38 (b, 1H), 8.19 (s, 1H), 7.45−7.18 (m, 10H), 6.87 (m, 4H), 6.37 (dd, ^3J = 7.0 and 6.5 Hz), 4.96 (m, 1H), 4.80 (d, 1H, ^2J = 15.0 Hz), 4.74 (d, 1H, ^2J = 15.0 Hz), 3.97−3.75 (m, 2H), 3.78 (s, 6H), 3.74−3.63 (m, 2H), 3.15 (d, 1H, ^2J = 10.0 Hz), 2.94 (d, 1H, ^2J = 10.0 Hz), 2.73 (m, 2H), 2.53 (ddd, 1H, ^2J = 14.0 Hz, ^3J = 6.5 and 4.5 Hz), 2.43 (m, 1H), 1.55 (s, 3H), 1.25−1.21 (m, 12H). ^{13}C NMR (125 MHz, CD_3CN) δ: 163.7, 158.9, 150.4, 144.5, 137.6 (q, *J* = 39 Hz), 135.8, 135.1, 134.9, 130.1, 128.0, 127.1, 125.9, 120.9 (q, *J* = 265 Hz), 118.6, 113.2, 110.6, 87.0, (85.4 and 85.3), 84.0, (74.7 and 74.6), 63.3, (58.5 and 58.3), 54.9, 51.9, (43.3 and 43.2), 38.3, (24.3 and 24.2), (23.91 and 23.85), (20.2 and 20.1), 11.3. ^{31}P NMR (200 MHz, CD_3CN) δ: 149.7. ^{19}F NMR (470 MHz, CD_3CN) δ: −63.28. HRMS (ESI-TOF) *m/z*: calcd for $C_{44}H_{51}F_3N_7NaO_8P$ $[M + Na]^+$ 916.3387, found 916.3387.

Oligonucleotide Synthesis. Oligonucleotides were synthesized on a 1.0 μmol scale using an automatic DNA/RNA synthesizer. Benzylthiotetrazole as an activator and coupling times of 20 and 300 s were used for the couplings of standard DNA and RNA building blocks, respectively. *Automatic coupling of* ***12***: A 0.13 mol L^{-1} solution of **12** was prepared and added to the synthesizer. The coupling time was increased to 600 s, and otherwise the standard coupling cycle was used. According to the DMTr assay, a 92% coupling efficiency was obtained. *Manual coupling of* ***12***: A 0.20 mol L^{-1} solution of **12** (10 μmol) was prepared. This solution and a solution of benzylthiotetrazole (0.25 mol L^{-1} in dry acetonitrile, 10 μmol) were suspended with the CPG support (bearing the sequence before **12**, 1 μmol). The suspension was mixed for 10 min under nitrogen at ambient temperature, loaded onto the synthesis column, and filtered. The synthesis column was set to the synthesizer, and then the chain elongation was continued automatically. According to the DMTr assay, nearly quantitative coupling of **12** was provided. After the chain elongation, the supports were suspended in concentrated ammonia (33% aqueous NH_3 at 55 °C overnight), the mixtures were filtered, and the filtrates were evaporated to dryness. The residues of oligodeoxyribonucleotides **ON1**−**ON5** and 2′-*O*-methyl oligoribonucleotide **ON6** were dissolved in water and subjected to RP HPLC purification. The residues of HIV-1-TAR models were dissolved in triethylamine trihydrofluoride (75 μL), triethylamine (60 μL), and DMSO (115 μL), mixed for 2.5 h at 65 °C, and filtered through an ion exchange cartridge, after which the filtrates were evaporated to dryness. The residues of the free RNAs were dissolved in sterilized water, and then RP HPLC was carried out. After RP HPLC purification using a semipreparative RP HPLC column (C-18, 250 mm × 10 mm, 5 μm) with gradient elution (0−90% acetonitrile in 0.1 mol L^{-1} triethylammonium acetate in 25 min) and detection at 260 nm, the homogenized oligonucleotides were lyophilized, and their authenticities were verified by MS (ESI-TOF) (Table 2).

Table 2. Observed and Calculated Molecular Masses of the Oligonucleotides Labeled with 6

entry	oligonucleotide	observed molecular mass	calculated average molecular mass
1	**ON1**	4514.8[a]	4515.0
2	**^{19}F-HIV-1 TAR^1**	9492.5[b]	9494.1
3	**^{19}F-HIV-1 TAR^2**	9492.3[b]	9494.1
4	**^{19}F-HIV-1 TAR^3**	9492.3[b]	9494.1

[a]Calculated from the most intense isotope combination at $[(M - 3H)]^{3-}/3$. [b]Calculated from the most intense isotope combination at $[(M - 11H)]^{11-}/11$.

^{19}F NMR Spectroscopy Studies. Oligonucleotides (as triethylammonium salts) were dissolved in an appropriate buffer [500 μL of either 10 mmol L^{-1} sodium phosphate, 2 mmol L^{-1} $MgCl_2$, 0.1 mol L^{-1} NaCl in D_2O−H_2O (1:9 v/v), pH 5.5; the same but at pH 6.0; or 10 mmol L^{-1} sodium cacodylate, 0.1 mol L^{-1} NaCl in D_2O−H_2O (1:9 v/v), pH 7.0]. All of the samples were heated to 90 °C and then allowed to cool to room temperature, after which the NMR measurements were carried out at target temperatures. Spectra were recorded at a frequency of 470.6 MHz on a Bruker Avance 500 MHz spectrometer. Typical experimental parameters were chosen as follows: ^{19}F excitation pulse, 4.0 μs; acquisition time, 1.17 s; prescan delay, 6.0 μs; relaxation delay, 0.8 s; usual number of scans, 2048 or 1024. The parameters were optimized to gain the signals with the longest relaxation rate (triplex). In order to improve the authenticity of the relative peak areas (spectra in Figures 3 and 4), the decrease (triplexes) and increase (single strand) in the peak areas were additionally referred to an internal standard (5-[4,4,4-trifluoro-3,3-bis(trifluoromethyl)but-1-ynyl]uridine)[12] as far as it was possible. A macro command was used for automatic temperature ramps using a 20 min equilibration time for each temperature.

Melting Temperature Studies. The melting curves (absorbance vs temperature) were measured at 260 nm on a PerkinElmer Lambda 35 UV−vis spectrometer equipped with a multiple cell holder and a Peltier temperature controller. The temperature was changed from 10 to 90 °C at a rate of 0.5 °C/min. The measurements were performed in 10 mmol L^{-1} sodium phosphate buffer (pH 6) containing 0.1 mol L^{-1} NaCl and 2 mmol L^{-1} $MgCl_2$ or in 10 mmol L^{-1} sodium cacodylate (pH 7) containing 0.1 mol L^{-1} NaCl. The oligonucleotides were used at a concentration of 2 μmol L^{-1}. Each T_m value was determined as the maximum of the first derivative of the melting curve.

dx.doi.org/10.1021/jo500326j | J. Org. Chem. 2014, 79, 3529−3536

■ ASSOCIATED CONTENT

Supporting Information

NMR spectra for **11** and **12**, RP HPLC profiles and MS (ESI-TOF) data for **ON1** and the labeled HIV-1 TAR models, and UV and CD data for the oligonucleotides. This material is available free of charge via the Internet at http://pubs.acs.org.

■ AUTHOR INFORMATION

Corresponding Author

*E-mail: pamavi@utu.fi.

Notes

The authors declare no competing financial interest.

■ ACKNOWLEDGMENTS

Financial support from the Academy of Finland (251539 and 256214) is gratefully acknowledged. We also thank Anu Kiviniemi for some preliminary work considered in this study.

■ REFERENCES

(1) Hammann, C.; Norman, D. G.; Lilley, D. M. *Proc. Natl. Acad. Sci. U.S.A.* **2001**, *98*, 5503.
(2) Olsen, G. L.; Edwards, T. E.; Deka, P.; Varani, G.; Sigurdsson, S. Th.; Drobny, G. P. *Nucleic Acids Res.* **2005**, *33*, 3447.
(3) Kreutz, C.; Kählig, H.; Konrat, R.; Micura, R. *J. Am. Chem. Soc.* **2005**, *127*, 11558.
(4) Kreutz, C.; Kählig, H.; Konrat, R.; Micura, R. *Angew. Chem., Int. Ed.* **2006**, *45*, 3450.
(5) Henning, M.; Munzarová, M. L.; Bermel, W.; Scott, L. G.; Sklenář, V.; Williamson, J. R. *J. Am. Chem. Soc.* **2006**, *128*, 5851.
(6) Graber, D.; Moroder, H.; Micura, R. *J. Am. Chem. Soc.* **2008**, *130*, 17230.
(7) Barhate, N. B.; Barhate, R. N.; Cekan, P.; Drobny, G.; Sigurdsson, S. Th. *Org. Lett.* **2008**, *10*, 2745.
(8) Henning, M.; Scott, L. G.; Sperling, E.; Bermel, W.; Williamson, J. R. *J. Am. Chem. Soc.* **2007**, *129*, 14911.
(9) Kiviniemi, A.; Virta, P. *J. Am. Chem. Soc.* **2010**, *132*, 8560.
(10) Tanabe, K.; Sugiura, M.; Nishimoto, S. *Bioorg. Med. Chem.* **2010**, *18*, 6690.
(11) Moumné, R.; Pasco, M.; Prost, E.; Lecourt, T.; Micouin, L.; Tisne, C. *J. Am. Chem. Soc.* **2010**, *132*, 13111.
(12) Kiviniemi, A.; Virta, P. *Bioconjugate Chem.* **2011**, *22*, 1559.
(13) Sakamoto, T.; Hayakawa, H.; Fujimoto, K. *Chem. Lett.* **2011**, *40*, 720.
(14) Sakamoto, T.; Shimizu, Y.; Sasaki, J.; Hayakawa, H.; Fujimoto, K. *Bioorg. Med. Chem. Lett.* **2011**, *21*, 303.
(15) Lombés, T.; Moumné, R.; Larue, V.; Prost, E.; Catala, M.; Lecourt, T.; Dardel, F.; Micoin, L.; Tisné, C. *Angew. Chem., Int. Ed.* **2012**, *51*, 9530.
(16) Fauster, K.; Kreutz, C.; Micura, R. *Angew. Chem., Int. Ed.* **2012**, *51*, 13080.
(17) Kiviniemi, A.; Murtola, M.; Ingman, P.; Virta, P. *J. Org. Chem.* **2013**, *78*, 5153.
(18) Tanabe, K.; Tsuda, T.; Ito, T.; Nishimoto, S. *Chem.—Eur. J.* **2013**, *19*, 15133.
(19) Chen, H.; Viel, S.; Ziarelli, F.; Peng, L. *Chem. Soc. Rev.* **2013**, *42*, 7971.
(20) Gerig, J. T. In *Biological Magnetic Resonance*; Berliner, L., Reuben, J., Eds.; Plenum Press: New York, 1978; p 139.
(21) Rastinejad, F.; Evilia, C.; Lu, P. *Methods Enzymol.* **1995**, *261*, 560.
(22) Gerig, J. T. *Prog. Nucl. Magn. Reson. Spectrosc.* **1994**, *26*, 293.
(23) Kitevski-LeBlanc, J. L.; Prosser, R. S. *Prog. Nucl. Magn. Reson. Spectrosc.* **2012**, *62*, 1.
(24) Markley, J. C.; Chirakul, P.; Sologub, D.; Sigurdsson, S. Th. *Bioorg. Med. Chem. Lett.* **2001**, *11*, 2453.
(25) Raunjær, M.; Bryld, T.; Wengel, J. *Chem. Commun.* **2003**, 1604.
(26) Wengel, J. *Acc. Chem. Res.* **1999**, *32*, 301.
(27) Pfundheller, H. M.; Bryld, T.; Olsen, C. E.; Wengel, J. *Helv. Chim. Acta* **2000**, *83*, 128.
(28) Ueno, Y.; Nagasawa, Y.; Sugimoto, I.; Kojima, N.; Kanazaki, M.; Shuto, S.; Matsuda, A. *J. Org. Chem.* **1998**, *63*, 1660.
(29) Wang, G.; Seifert, W. E. *Tetrahedron Lett.* **1996**, *37*, 6515.
(30) Fensholdt, J.; Thrane, H.; Wengel, J. *Tetrahedron Lett.* **1995**, *36*, 2535.
(31) Thrane, H.; Fensholdt, J.; Regner, M.; Wengel, J. *Tetrahedron* **1995**, *51*, 10389.
(32) Maag, H.; Schmidt, B.; Rose, S. J. *Tetrahedron Lett.* **1994**, *35*, 6449.
(33) Kiviniemi, A.; Virta, P.; Lönnberg, H. *Bioconjugate Chem.* **2008**, *19*, 1726.
(34) Kiviniemi, A.; Virta, P.; Lönnberg, H. *Bioconjugate Chem.* **2010**, *21*, 1890.
(35) Abboud, J.-L. M.; Foces-Foces, C.; Notario, R.; Trifonov, R. E.; Volovodenko, A. P.; Ostrovskii, V. A.; Alkorta, I.; Elguero, J. *Eur. J. Org. Chem.* **2001**, 3013.
(36) Stepanova, N. P.; Galishev, V. A.; Turbanova, E. S.; Maleev, A. V.; Potekhin, K. A.; Kurkutova, E. N.; Struchkov, Y. T.; Petrov, A. A. *Zh. Org. Khim.* **1989**, *25*, 1613.
(37) Rostovtsev, V. V.; Green, L. G.; Fokin, V. V.; Sharpless, K. B. *Angew. Chem., Int. Ed.* **2002**, *41*, 2596.
(38) O-Yang, C.; Kurz, W.; Eugui, E. M.; McRoberts, M. J.; Verheyden, J. P. H.; Kurz, L. J.; Walker, K. A. M. *Tetrahedron Lett.* **1992**, *33*, 41.
(39) Jones, G. H.; Taniguchi, M.; Teggs, D.; Moffatt, J. G. *J. Org. Chem.* **1979**, *44*, 1309.
(40) Wu, T.; Nauwelaerts, K.; Van Aerschot, A.; Froeyen, M.; Lescrinier, E.; Herdewijn, P. *J. Org. Chem.* **2006**, *71*, 5423.
(41) Arya, D. P.; Micovic, L.; Charles, I.; Coffee, R. L., Jr.; Willis, B.; Xue, L. *J. Am. Chem. Soc.* **2003**, *125*, 3733.
(42) Arya, D. P.; Xue, L.; Tennant, P. *J. Am. Chem. Soc.* **2003**, *125*, 8070.
(43) Arya, D. P. *Acc. Chem. Res.* **2011**, *44*, 134.
(44) Charles, I.; Xi, H.; Arya, D. P. *Bioconjugate Chem.* **2007**, *18*, 160.
(45) Ketomäki, K.; Virta, P. *Bioconjugate Chem.* **2008**, *19*, 766.